Comparison of atomistic and continuum theoretical approaches to determine electronic properties of GaN/AlN quantum dots

Oliver Marquardt,[1,*] Daniel Mourad,[2] Stefan Schulz,[2,†] Tilmann Hickel,[1] Gerd Czycholl,[2] and Jörg Neugebauer[1]
[1]*Max-Planck Institut für Eisenforschung, Max-Planck-Straße 1, D-40237 Düsseldorf, Germany*
[2]*Institute for Theoretical Physics, University of Bremen, D-28359 Bremen, Germany*
(Received 16 September 2008; revised manuscript received 29 October 2008; published 1 December 2008)

In this work we present a comparison of multiband $\mathbf{k}\cdot\mathbf{p}$ models, the effective-bond-orbital approach, and an empirical tight-binding model to calculate the electronic structure for the example of a truncated pyramidal GaN/AlN self-assembled quantum dot with a zinc-blende structure. For the system under consideration, we find very good agreement between the results of the microscopic models and the eight-band $\mathbf{k}\cdot\mathbf{p}$ formalism, in contrast to a 6+2-band $\mathbf{k}\cdot\mathbf{p}$ model, where conduction band and valence band are assumed to be decoupled. This indicates a surprisingly strong coupling between conduction- and valence-band states for the wide-band-gap materials GaN and AlN. Special attention is paid to the possible influence of the weak spin-orbit coupling on the localized single-particle wave functions of the investigated structure.

DOI: 10.1103/PhysRevB.78.235302 PACS number(s): 71.15.−m, 73.21.La, 73.22.Dj

I. INTRODUCTION

Nitride-based semiconductor nanostructures are promising materials due to their potential application in optoelectronic and high-power or high-temperature electronic devices.[1] AlN, GaN, and InN and their ternary and quaternary alloys in principle allow the emission of the whole spectrum of visible light from red to ultraviolet. Within the past years, increasing research interest has been on the investigation of GaN/AlN quantum dots (QDs) in order to develop single-electron transistors,[2] ultraviolet sources,[3] and detectors.[4]

Group-III nitrides can crystallize in the thermodynamically stable configuration with a wurtzite crystal structure and in the metastable modification with a zinc-blende structure.[5] The great majority of wurtzite GaN/AlN QDs are grown along the polar [0001] direction. These structures exhibit large spontaneous and strain-induced polarization. These effects lead to a large internal electrostatic field, which is very unique to III-nitride heterostructures and has a significant effect on the electronic and optical properties of QDs. The magnitude of the electrostatic built-in field has been estimated to be on the order of MV/cm.[6,7] Such fields spatially separate the electrons and holes, which leads to a reduction in the oscillator strength and enhanced radiative lifetimes.[7–9]

In contrast, in the cubic GaN/AlN QD structures, the spontaneous polarization is absent due to the higher crystal symmetry.[10] Furthermore, experimental data indicate that the piezoelectric contributions are small.[11] Therefore, GaN/AlN QDs with a zinc-blende structure are expected to have advantages in optoelectronic devices. Recently, there has been an increasing interest in cubic GaN/AlN QDs due to the improvement of their growth process.[7,11–15] In order to understand the optical properties of cubic GaN/AlN QDs, the investigation of the electronic structure of these structures is of major importance. For instance, the excitation energies and wave functions are crucial ingredients for carrier-carrier[16] and carrier-phonon[17] scatterings in nitride QD structures.

Different approaches have been developed to calculate the electronic structure of semiconductor QDs. These methods range from continuum approaches such as effective-mass[18–20] and $\mathbf{k}\cdot\mathbf{p}$ (Refs. 8 and 21–23) approximations to atomistic models, e.g., tight-binding (TB) (Refs. 24–26) and pseudopotential approaches.[27–29] The number of available theoretical models for the calculation of the electronic structure makes an evaluation of these methods with respect to the accuracy of the investigated material properties necessary.

While in atomistic descriptions the computational effort grows with the number of involved atoms, the accuracy of continuum models decreases when the structure's characteristic dimensions reach the length scale of the atomic bonds. On the other hand, the continuum models are not limited to a maximum size of the structure. Previously, different $\mathbf{k}\cdot\mathbf{p}$ models have been compared with an atomistic empirical pseudopotential method for different semiconductor systems.[28,30,31] These investigations revealed various shortcomings in the continuum models resulting from the lack of atomistic description or an insufficient number of involved bands. However, a comparison of atomistic and continuum models employing the same number of involved bands is essential in order to determine the accuracy of computationally less demanding models.

In this work, we perform a careful comparison of various atomistic and continuum methods, namely, an empirical tight-binding model (ETBM), an effective bond-orbital model (EBOM), and two variations of the $\mathbf{k}\cdot\mathbf{p}$ approach, to calculate the electronic structure of GaN/AlN QDs with a zinc-blende structure. Since we use for all methods an equivalent set of input parameters, the outputs of the various approaches can be compared directly. We focus our attention on the differences in the electron and hole wave functions and the corresponding single-particle energies. A comparison of optical properties such as excitonic absorption or emission spectra, which can be obtained in the framework of a full configuration scheme,[32] is beyond the scope of present work.

In this study special attention is paid to the influence of the small spin-orbit coupling on the results, an effect which has been commonly neglected in III-nitride QD systems.[8,23,24,33–36] However, recent investigations on wurtz-

ite III-nitride QDs show that neglecting the spin-orbit coupling leads to artificial degeneracies of hole states.[37,38] The influence of spin-orbit coupling on the properties of nanostructures can be expected to be strongly nonlinear in empirical approaches, as it enters both the common bulk parameter set and the geometry-related part of the Hamiltonian. The influence of the conduction band (CB)–valence band (VB) coupling in the eight-band $\mathbf{k}\cdot\mathbf{p}$ model will be shown to have a surprisingly large effect on the electron binding energies despite the fact that GaN is a wide-band-gap material.

This paper is organized as follows. In Sec. II, we introduce the applied methods and their underlying concepts and approximations. Section III is dedicated to the GaN/AlN QD geometry. Section IV deals with the electronic structure of these systems. The influence of the spin-orbit coupling will be discussed in detail in Sec. IV B. In Sec. IV C we compare the results of the six- and the eight-band $\mathbf{k}\cdot\mathbf{p}$ models.

II. APPLIED METHODS

While atomistic models of different sophistication approaching the electronic properties of semiconductor nanostructures lead to an increasing computational effort with the number of involved atoms, continuum models may produce strong deviations from results obtained in atomistic simulations. These deviations are expected to increase with decreasing characteristic dimensions of the structure. The aim of this paper is to provide a comparison of complementary approaches to the electronic structure of GaN/AlN QDs in a cubic structure.

Previous studies compared the $\mathbf{k}\cdot\mathbf{p}$ formalism with highly accurate but computationally expensive empirical pseudopotential calculations.[30,39] In this study we chose two microscopic approaches with various levels of approximation which have been constructed such that they reproduce the band structure in the optical application–relevant region around the Γ point. The investigated methods are: (i) the ETBM, (ii) the EBOM, and (iii) the $\mathbf{k}\cdot\mathbf{p}$ formalism employing different numbers of bands. The choice of equivalent input parameters in the investigated methods allows a direct comparison of differences resulting purely from the different levels of approximation. While the ETBM is the most accurate model among the investigated ones, the EBOM and the $\mathbf{k}\cdot\mathbf{p}$ formalism allow a straightforward study of different material parameters on the electronic structure as the input parameter set is fixed for the investigated material system. In this section, we will introduce the investigated methods used to compute the electronic structure of the model system.

A. ETBM

The key assumption of the tight-binding method is that the overlap of atomic orbitals decreases rapidly with the distance of their corresponding atoms; i.e., only Hamilton matrix elements (TB parameters) between neighboring atoms (typically up to the second- or third-nearest-neighbor shell) have to be included. For the polar semiconductors GaN and AlN considered in this study, the upper valence band is mainly formed by the p orbitals of the anions and the conduction band from the s orbitals of the cations.[40] We therefore apply an $s_c p_a^3$ TB model,[26] where each anion is described by the outer valence orbitals per spin direction: p_x, p_y, and p_z. The cations are modeled by a single s orbital per spin direction. Overlap matrix elements up to the second-nearest neighbors are included in our TB model. Following Ref. 41, the spin-orbit component of the bulk Hamiltonian H^{bulk} couples only p orbitals at the same atom. By analytical diagonalization of the TB Hamiltonian H^{bulk} for special $\mathbf{k}$ directions, the electronic dispersion is obtained as a function of the TB parameters. Equations for the TB parameters can now be deduced in terms of the Kohn-Luttinger parameters $(\gamma_1,\gamma_2,\gamma_3)$, the single-particle energy gap E_g, the effective electron mass m_e, and the spin-orbit splitting Δ_{so} at the Γ point. Doing so, one TB parameter has to be determined self-consistently to reproduce the L-point energy of the split-off band. This parametrization has been verified to correctly describe the band-structure region around the Γ point. Since we are dealing with the electronic properties of a nanostructure formed from a direct-gap semiconductor material here, mainly this part of the bulk band structure is of importance. Furthermore, due to the large energetic splitting (>1 eV) between the zone center (Γ point) and the side valleys (L and X points), the quantum confinement will not introduce a mixing between these states. Therefore, the region around the Γ point is expected to dominate the QD states.

B. EBOM

In the EBOM the TB orbitals are replaced by so-called *effective orbitals* located on the sites of the underlying lattice, thus neglecting the atomic basis of the material. With respect to the zinc-blende structure which is considered in this study, the underlying symmetry of the original crystal structure is changed to that of an fcc lattice with effective orbitals

$$|\mathbf{R},i,\sigma\rangle_{\mathrm{eff}},\quad i=s,p_x,p_y,p_z,\quad \sigma=\uparrow,\downarrow, \tag{1}$$

on each Bravais lattice site $\mathbf{R}$. We note that this approximation gives rise to an artificial change in the symmetry from T_d (zinc blende) to O_h (fcc).

An advantage of the EBOM approach is that it allows us to directly relate the underlying TB parameters with the corresponding $\mathbf{k}\cdot\mathbf{p}$ Hamiltonian. A self-consistent fitting of the ETBM parameters to the bulk band structure is therefore not needed.

A first EBOM parametrization by Chang[42] incorporated three-center overlap integrals. This parametrization was restricted to coupling up to nearest neighbors only, so that solely the Γ-point energies could be fitted to the set of $\mathbf{k}\cdot\mathbf{p}$ parameters. In the present work, we use the parametrization of Loehr,[43] which includes hopping up to second-nearest neighbors to fit the band structure of the bulk material to the above-mentioned set of parameters. This parametrization additionally allows for a fit to the X-point energies of the conduction band (X_{1c}), the degenerate heavy hole or light hole band (X_{5v}), and the split-off band (X_{3v}). The degeneracy of the hh or lh band at X is subsequently lifted by the incorporation of spin-orbit coupling into the TB Hamiltonian.

TABLE I. Material parameters for zinc-blende GaN and AlN (Refs. 8 and 49).

Parameter	GaN	AlN
a (Å)	4.5	4.38
E_g (eV)	3.26	4.9
ΔE_{vb} (eV)	0.8	0.0
X_1^c (eV)	4.428	5.346
X_3^v (eV)	−6.294	−5.388
X_5^v (eV)	−2.459	−2.315
E_P (eV)	25.0	27.1
Δ_{so} (eV)	0.017	0.019
m_e (m_0)	0.15	0.25
γ_1	2.67	1.92
γ_2	0.75	0.47
γ_3	1.10	0.85

C. k·p method

In the **k**·**p** formalism the wave functions are replaced by their envelope which no longer resolves individual atoms. By this coarse-graining treatment it becomes possible to describe the electronic structure very efficiently on a continuum scale. Within this work, we calculate the electronic structure in a basis set of eight complex envelope eigenfunctions. This results in an eight-band **k**·**p** Hamiltonian,[44] given in the Appendix. The eight-band formalism can be reduced to two plus six bands if the Kane parameter E_P describing the coupling between the VB and the CB is set to zero (see the Appendix). Taking this parameter into account causes modifications of the effective mass and Luttinger parameters as well as additional coupling elements U and V within the Hamiltonian matrix $H^{8\times8}$, which are neglected in the 6+2-band model. Another common simplification which will be checked explicitly in this study is to neglect the spin-orbit coupling parameter Δ_{so} which is on the order of a few meV in the III-nitride systems.[45] This approximation reduces the dimensionality of the Hamiltonian and thus the computational effort. The computation of the **k**·**p** electron and hole wave functions is performed in the plane-wave formalism within the S/PHI/nX software package.[46,47]

D. Comparison of the bulk band structure

For the parametrization of the bulk band structure, we use a set given by Fonoberov and Balandin,[8] which has been shown to accurately reproduce experimental data and recent G_0W_0 calculations[48] around the Γ point. The parameter sets are given in Table I. Figure 1 shows the resulting band structure along the L-Γ-X path for the three methods. As can be seen, the agreement around the Γ point is perfect, whereas expected clear deviations arise toward the Brillouin-zone boundaries.

The EBOM reproduces the bulk GaN valence-band structure obtained from previous work[49] throughout the Brillouin zone. The ETBM results along the Γ-L direction are in excellent agreement with the EBOM valence-band structure,

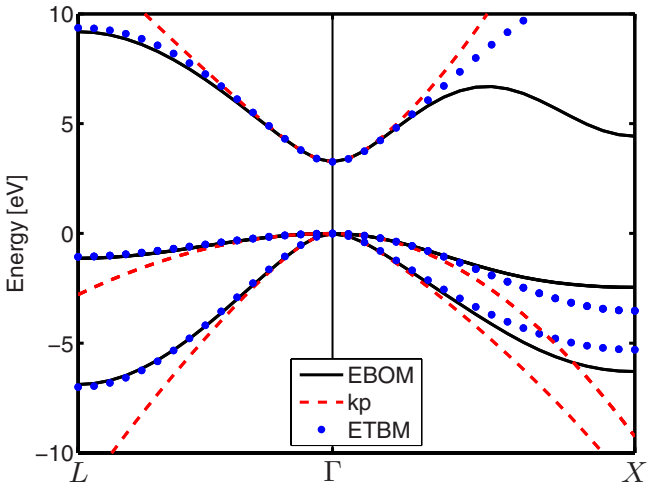

FIG. 1. (Color online) Bulk band structure of zinc-blende GaN in two high-symmetry directions calculated by the effective-bond-orbital method (solid lines), the $s_c p_a^3$ tight-binding model (dotted lines), and the eight-band **k**·**p** approach (dashed lines).

while slight deviations from the EBOM results are observed at the X point. Remember that the EBOM energies have been fitted to this point of the Brillouin zone.

Furthermore, the EBOM accurately describes the conduction band along the Γ-X direction. In particular, an additional maximum along the Γ-X direction is reproduced in agreement with *ab initio* band-structure calculations.[49] The ETBM conduction band deviates from the EBOM results near the X point since higher conduction bands are not taken into account.

In contrast to the EBOM and ETBM, the eight-band **k**·**p** reproduces the band structure only for small **k** vectors around Γ. Similar to the discussion of the ETBM, by taking more bands into account, better agreement of the **k**·**p** band structure throughout the Brillouin zone can be achieved.[50]

However, in the present study we refrain from such an extended **k**·**p** or TB Hamiltonian to keep the numbers of involved bands equal and thus consistent within the investigated models. Furthermore, in accordance with the discussion in Sec. II A, the Γ-point character is expected to dominate the single-particle states in a nanostructure with characteristic dimensions of only a few nanometers. Indeed, as will be shown later, even the 8×8 **k**·**p** Hamiltonian and the $s_c p_a^3$ TB model are excellent approximations.

III. MODEL QUANTUM DOT

Cubic GaN QDs embedded in AlN have been experimentally investigated by various groups.[7,11–15] These studies have shown that such QDs grow as truncated pyramidal structures.[11,12] The QDs are commonly grown in a Stranski-Krastanov growth mode; i.e., they form spontaneously when the wetting layer (WL) exceeds a critical thickness.

As pointed out before a major aim of this work is to investigate the consistence of the results obtained by the continuum **k**·**p** approach with the outcomes of (semi)microscopical tight-binding approaches explained in Sec. II. While

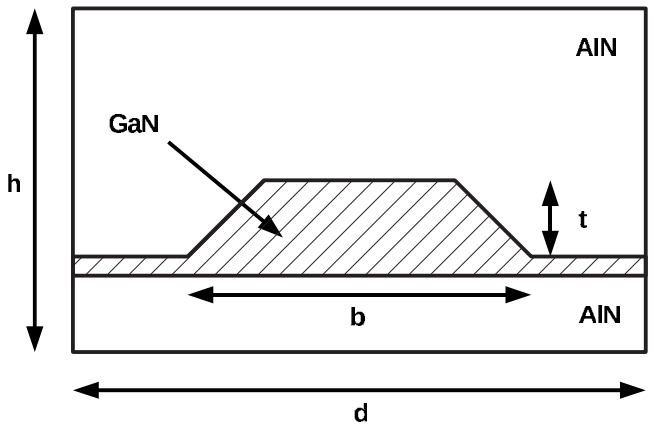

FIG. 2. Schematic geometry of our model quantum dot. The base length b and the height t of the pyramidal frustum determine the dot size, while h and d define the size of the supercell.

the accuracy of the continuum $\mathbf{k}\cdot\mathbf{p}$ model is known to increase with the dimensions of the structure, a comparison between continuum and atomistic simulations is highly interesting for systems with characteristic dimensions in the order of magnitude of the bulk lattice constants. Furthermore, the small number of involved atoms also limits the computational effort of the atomistic calculations.

As a test quantum dot we therefore consider a truncated pyramid with a square base length of $b=16a$ and a height of $t=4a$ only (Fig. 2). It is placed on top of a GaN WL with a thickness of $0.5a$, where a is the AlN lattice constant. This corresponds to $t\approx 1.75$ nm and $b=7$ nm. The dot is oriented along the [001] axis. Previous studies of GaN/AlN QDs with a wurtzite structure showed no intermixing between Ga and Al in these structures.[51,52] Since the structural properties of cubic GaN QDs embedded in AlN are found to be similar to those of the hexagonal ones,[11] we also take in our simulations the compositions of the nanostructure and the surrounding barrier material to be pure GaN and AlN, respectively. Only for the WL composition experimentally a weak interdiffusion of Ga and Al atoms is found.[52] Since the focus of this study is on the bound single-particle states, which are localized inside the nanostructure, compositional fluctuations in the WL region have only minor influence on the bound single-particle states and will be neglected. Note that the symmetry of the outer shape of the QD resulting from the confinement potential is a C_{4v} symmetry, while the underlying crystal lattice lacks inversion symmetry and reduces the symmetry to C_{2v}.

Within all three approaches, the QD is located in a sufficiently large supercell to eliminate the influence of the chosen supercell boundaries on the single-particle states. The convergence of the eigenstates with respect to the supercell size has been carefully checked.

In the framework of an $s_c p_a^3$ TB model, the C_{2v} symmetry of the QDs underlying zinc-blende structure is naturally included. To set up the Hamiltonian we use the TB parameters of the corresponding bulk materials. At the GaN/AlN interfaces we use a linear interpolation of the TB parameters of GaN and AlN. Since the nitrogen atoms form a common anion lattice, the interpolation affects only second-nearest-neighbor elements which are small compared to the nearest-neighbor contributions.

The application of EBOM to describe QDs is similar to the ETBM approach. The main difference is the restriction to a slightly more coarse-grained grid where the anion and cation positions cannot be resolved. This coarse graining changes the underlying lattice from zinc blende to fcc. Therefore, this approach cannot sustain the original C_{2v} symmetry of the zinc-blende structure and increases the number of symmetry operations. In this case we are left with a C_{4v} symmetry.

Within the $\mathbf{k}\cdot\mathbf{p}$ formalism, the dot and the WL are described by a spatially resolved envelope function. We use the bulk GaN parameter set inside the nanostructure and bulk AlN parameters for the matrix material. The $\mathbf{k}\cdot\mathbf{p}$ formalism does not resolve individual atoms and will therefore not reproduce the C_{2v} symmetry of the underlying zinc-blende lattice. The QD is simulated on a real-space mesh of $80\times 80\times 80$ mesh points.

In this study the focus is on a systematic comparison of the different approaches introduced in Sec. II rather than on a complete description of all aspects of a QD. Therefore, we do not consider contributions from strain and electrostatic built-in fields in our calculations. Nevertheless, as we will discuss in Sec. IV, our results for the single-particle level structure are in qualitative agreement with results obtained in Ref. 8, where strain effects and piezoelectric fields were explicitly taken into account.

IV. ELECTRONIC PROPERTIES OF CUBIC GaN QUANTUM DOTS

A. Single-particle energies and states

Using the above quantum-dot geometry, we applied the three approaches to compute the bound hole and electron states. In all three approaches, we consistently find a total number of eight bound electron states. Due to the large effective mass of the hole states and the large valence-band offset, the number of localized hole states is much higher. While higher excited states play an important role in carrier-carrier and carrier-phonon interactions, we will restrict our discussion on the first four bound electron and hole states since these dominate the excitonic and absorption processes in QD structures. The energy levels of these states as calculated by the three approaches are shown in Fig. 3.

Figure 4 shows a top view of the QD geometry and the modulus square $|\psi(\mathbf{r})|^2$ of the first four single-particle wave functions for electrons and holes. Each state is twofold degenerate due to time-reversal symmetry. Qualitatively comparable results were found by Fonoberov and Balandin[8] for larger truncated pyramidal GaN/AlN zinc-blende QDs.[8]

1. Electron states

Comparing the three approaches, the single-particle states for the electrons are quantitatively as well as qualitatively very similar: both their energy eigenvalues and the corresponding symmetry characters agree well. According to their nodal structure, these states can be classified as s-, p_x-, p_y-,

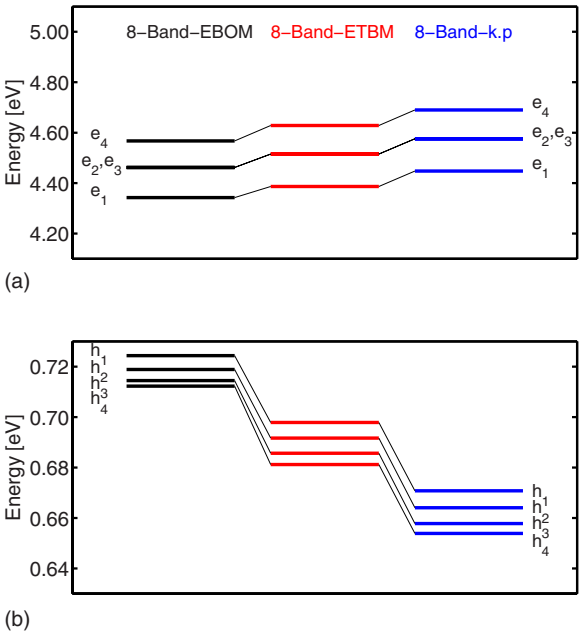

FIG. 3. (Color online) The first four electron and hole single-particle energy levels of the GaN QD, as calculated by the EBOM, the $s_c p_a^3$ ETBM, and the eight-band $\mathbf{k}\cdot\mathbf{p}$ approach. All energies are given with respect to the valence-band edge of the AlN. Please note the different scalings for the electron and hole energies.

and d-like states. The electron ground state ψ_1^e is s-like, while the next two states are p-like. In the case of the $\mathbf{k}\cdot\mathbf{p}$ and the EBOM approach, the symmetry of the system is C_{4v}. Here, the atomic structure of the underlying zinc-blende lattice is not resolved, and the states ψ_2^e and ψ_3^e are energetically degenerate and form linear combinations of the form $p_\pm = (1/\sqrt{2})(p_x \pm i p_y)$. However, if taking the crystal structure into account, as it is done in an empirical TB model or a pseudopotential approach, the symmetry is reduced and degeneracies are lifted. For the QD considered here, a truncated pyramidal GaN QD grown along the [001] direction and with zinc-blende structure, the symmetry is C_{2v}. This symmetry lifts the equivalence between the [110] and $[1\bar{1}0]$ directions. Employing the empirical TB model, we therefore obtain energetically nondegenerate p_x- and p_y-like states for ψ_2^e and ψ_3^e, respectively. The states ψ_2^e and ψ_3^e are found to be nondegenerate with an energy difference of about 0.2 meV.

This value is much smaller than the energy differences between the lower bound states (see Fig. 3). This splitting may become more pronounced in other material systems or for other QD geometries.[29] Furthermore, inclusion of an atomistic strain field and the piezoelectric potential may also increase this splitting.[29]

2. Hole states

In contrast to the electron states, the hole states cannot be easily classified according to their nodal structure. This is due to the strong intermixing of the various valence bands and prevents a strict classification of the optical selection rules on total angular momentum selection rules. This finding emphasizes the importance of a multiband approach.

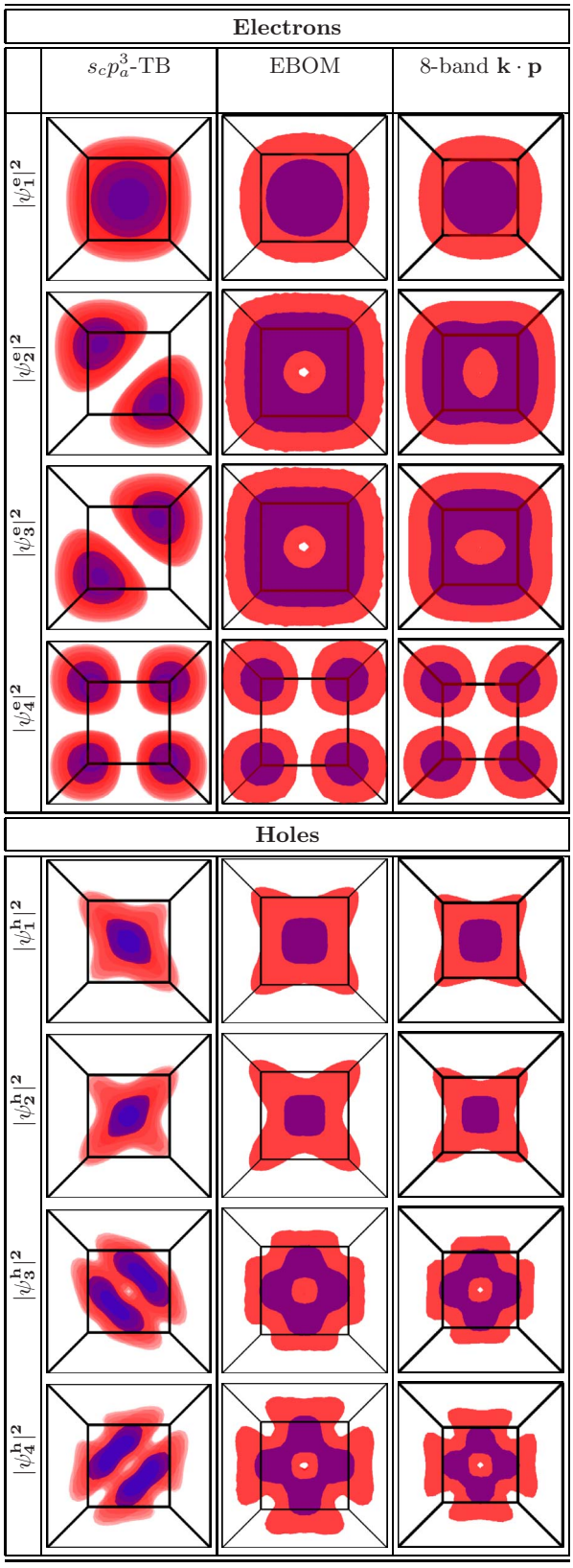

FIG. 4. (Color online) Top view of the truncated pyramidal GaN QD structure with the first four bound states for electrons (upper part) and holes (lower part). Depicted are isosurfaces of the probability density with 10% (red) and 50% (blue) of the maximum value.

Qualitatively, we find excellent agreement of the first four hole states, and again the corresponding eigenvalues for all three approaches lie within a narrow energy range. However, in the case of the eight-band $\mathbf{k}\cdot\mathbf{p}$ approach and the EBOM, the first two hole states ψ_1^h and ψ_2^h reveal no spatial anisotropy along the [110] and $[1\bar{1}0]$ directions, respectively. In the ETBM these states show a strong anisotropy along the [110] and $[1\bar{1}0]$ directions. This behavior again reflects that only the ETBM approach correctly reproduces the C_{2v} symmetry of the system. Note that the first two hole states are not degenerate, and all three approaches yield a splitting of about 6 meV. This effect results (mainly) from the spin-orbit splitting energy Δ_{so} and will be discussed in more detail in Sec. IV B.

The splitting of the first two hole states and the anisotropy of these states also have a strong influence on the optical properties of these systems. For example, the splitting of the states ψ_1^h and ψ_2^h may lead to additional lines in the optical spectra. Furthermore, the absence of spatial anisotropy of the states ψ_1^h and ψ_2^h may also lead to a vanishing polarization anisotropy λ for dipole transitions along directions [110] and $[1\bar{1}0]$, respectively. Energy differences in the absolute eigenvalues of electron and hole states occur due to the different representations of the structure within the investigated models, e.g., within the $\mathbf{k}\cdot\mathbf{p}$ formalism the mesh discretization cannot resolve the microscopic representation (i.e., the atomistic nature of the interface) of the other two methods. Shifting the QD boundaries slightly by ± 3.5 Å in the $\mathbf{k}\cdot\mathbf{p}$ formalism modifies the absolute energies of electron and hole states about ± 15 meV but causes no significant deviations in the energy difference of the states with respect to the corresponding ground state. Since the electron and hole level structure obtained here from the different approaches is found to be similar to the ones in Ref. 9 for a wurtzite InN/GaN QD, similar excitonic and emission spectra are expected for the present system. Selection rules for optical transitions can be analyzed in an analogous manner from symmetry aspects, as, for example, discussed in Ref. 9.

B. Influence of spin-orbit splitting

The spin-orbit coupling has been commonly neglected in previous studies of nitride-based nanostructures[8,23,24,33–36] since in group-III nitrides this contribution is on the order of a few meV.[45] The spin-orbit splitting is a relativistic effect which increases with the atomic number of the atoms.[53] For example, for CdSe and ZnSe this splitting is on the order of 0.4 eV.[26] Previous ETBM studies of CdSe/ZnSe QDs comparable in shape and size reveal a splitting in the first two hole states of several meV.[26,54] Without spin-orbit coupling these states are degenerate in the framework of a continuum approach, similar to the results reported in Ref. 8 for a truncated pyramidal GaN QD with a zinc-blende structure. Recently, the influence of the spin-orbit coupling was shown to break the degeneracy of the first two hole states in wurtzite InN/GaN QDs.[37,38] In this section we will therefore discuss the influence of the spin-orbit coupling on the electronic properties.

TABLE II. Single-particle energies for the truncated pyramidal GaN QD with ($\Delta_{so} \neq 0$) and without ($\Delta_{so}=0$) spin-orbit coupling. Each of the given states is twofold degenerate due to spin and time-reversal symmetry, respectively.

$\Delta_{so}=0$				
	3+1-band $\mathbf{k}\cdot\mathbf{p}$	Four-band $\mathbf{k}\cdot\mathbf{p}$	EBOM	ETBM
e_1 (eV)	4.5259	4.4477	4.3428	4.4246
e_2 (eV)	4.6768	4.5759	4.4621	4.5677
e_3 (eV)	4.6768	4.5759	4.4621	4.5677
e_4 (eV)	4.8069	4.6897	4.5670	4.6944
h_1 (eV)	0.6679	0.6726	0.7264	0.7070
h_2 (eV)	0.6679	0.6726	0.7264	0.7063
h_3 (eV)	0.6622	0.6627	0.7193	0.6962
h_4 (eV)	0.6558	0.6591	0.7172	0.6906
$\Delta_{so}=17$meV				
	6+2-band $\mathbf{k}\cdot\mathbf{p}$	Eight-band $\mathbf{k}\cdot\mathbf{p}$	EBOM	ETBM
e_1 (eV)	4.5259	4.4479	4.3429	4.3866
e_2 (eV)	4.6768	4.5761	4.4623	4.5152
e_3 (eV)	4.6768	4.5761	4.4623	4.5154
e_4 (eV)	4.8069	4.6900	4.5672	4.6284
h_1 (eV)	0.6677	0.6708	0.7244	0.6979
h_2 (eV)	0.6614	0.6641	0.7189	0.6917
h_3 (eV)	0.6570	0.6578	0.7145	0.6857
h_4 (eV)	0.6505	0.6539	0.7123	0.6812

In Table II the first four electron and hole energies for all three models are given in the presence as well as in the absence of spin-orbit coupling. Interestingly, the essential Kramers degeneracy resulting in twofold-degenerate states left aside, all calculations in the present paper bear a lift of degeneracy between the first two hole states of about 5–6 meV for the GaN dots, thus on the same order of magnitude as in the CdSe dots when spin-orbit coupling is included.[26] Since the EBOM parameters are not updated in a self-consistent manner, these models provide the opportunity to study the influence of the SO coupling Δ_{so} on the single-particle states and energies by gradually increasing this parameter from zero (which gives the limit of a four-band model) up to the final values of 17 meV in GaN and 19 meV in AlN.

The calculated dependence of the level splitting $\Delta_{h_2-h_1}$ as a function of Δ_{so} is given in Fig. 5. It is linear over the entire range. As the bulk band structures of GaN and AlN are hardly altered by the relatively small spin-orbit coupling, the main influence on the energy levels stems from the site-diagonal incorporation of the spin-orbit coupling into the nanostructure Hamiltonian. Additional $\mathbf{k}\cdot\mathbf{p}$ calculations give comparable results which are also depicted in Fig. 5. Hence, we have demonstrated that for the system under consideration, despite its relatively small influence on the bulk band structure, the inclusion of SO coupling allows us to lift the artificial degeneracy of hole states and therefore is of essen-

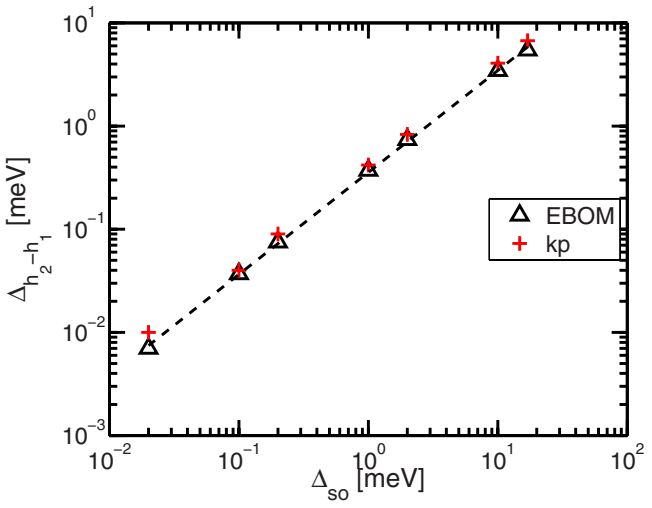

FIG. 5. (Color online) Energy difference $\Delta_{h_2-h_1}$ between the first two hole states in dependence on artificially varied spin-orbit coupling as calculated with the EBOM and the $\mathbf{k}\cdot\mathbf{p}$ model. The parameter Δ_{so} goes over several orders of magnitude; note the logarithmic scale, from 0 to an upper value given by $\Delta_{so}=17$ meV for GaN. The level splitting depends almost linearly on the bulk spin-orbit splitting.

tial importance for an accurate description of the single-particle states.

C. Influence of CB-VB coupling

While the eight-band formalism yields good agreement with the (semi)microscopic EBOM and ETBM methods, a six-band approach combined with an effective-mass model provides reliable information for the hole states only. Previous studies[21,55] found a strong influence of conduction band–valence band coupling for small- and medium-band-gap materials. Despite the fact that GaN has a large band gap of 3.26 eV, an unexpectedly large coupling is also observed for the system considered here: coupling effects between the conduction and valence bands significantly modify the electron binding energies. The corresponding values are given in Table II. However, these couplings have essentially no effect on the nodal character of the wave functions. Comparing the difference between the second and third electron state binding energies to the ground-state energy, we find 0.1282 eV applying the eight-band model, which is in excellent agreement with results from ETBM (0.1286 and 0.1288 eV) and EBOM (0.1194 eV) calculations. The 6+2-band $\mathbf{k}\cdot\mathbf{p}$ approach, which is for the electrons essentially an effective-mass approach, gives an energy difference of 0.1509 eV; i.e., it overestimates these energies by about 23 meV (17%). The origin of the rather large deviation is due to the value of the Kane matrix parameter E_P, which describes the CB-VB mixing effects and contains the respective dipole matrix element. Its value is large enough (E_P is 25 eV in GaN and 27.1 eV in AlN) to produce non-negligible coupling effects even for these wide-band-gap materials. This emphasizes the fact that not only the energy gap is important for a possible decoupling of the conduction and valence bands, but also the magnitude of the Kane parameter is of crucial importance.

Neglecting the spin-orbit coupling in the 6+2-band approach leads to a 3+1-band model. The energies are given in Table II. While the electron binding energies remain unchanged, we find a similar behavior for the hole states as we find using the four-band model by neglecting Δ_{so} in the eight-band model: the first two hole states are found to be degenerate in this model. When including the spin-orbit coupling, the resulting energy differences between the first and the second hole states are 6.3 meV in the 6+2-band approach and 6.7 meV within the full eight-band approach. For the hole states, only small differences between the eight- and the six-band models are found. Again, we find that the nodal character for the hole state wave functions as found by the eight-band model is preserved when neglecting E_P.

V. SUMMARY AND DISCUSSION

In conclusion, we applied atomistic and continuum models, namely, $\mathbf{k}\cdot\mathbf{p}$ models of different levels of sophistication and an EBOM and an $s_c p_a^3$ ETBM model, to derive the electronic properties of a zinc-blende GaN/AlN quantum dot. Starting from a set of equivalent parameters fitted to the bulk band structure around the Γ point for all methods and applying them to the same QD model structure, we find satisfactory agreement between the investigated models for the electron and hole wave functions and binding energies. This demonstrates that for the GaN/AlN system the semimicroscopic EBOM and the continuum eight-band $\mathbf{k}\cdot\mathbf{p}$ model are also appropriate to describe the electronic properties of nanostructures down to feature sizes of a few nanometers. Small discrepancies between the ETBM on one side and the EBOM and eight-band $\mathbf{k}\cdot\mathbf{p}$ models on the other side are found to be a result of the underlying crystal symmetry described correctly in the ETBM only.

Despite the large band gap of GaN and AlN, we find strong deviations of the electron binding energies between the eight-band model and a decoupled 6+2-band approach. These occur due to the strong influence of the Kane parameter E_P even in wide-band-gap materials.

The commonly neglected spin-orbit splitting parameter Δ_{so} lifts the degeneracy of the first two hole states. Even though Δ_{so} is much smaller in GaN and AlN than in, e.g., CdSe, the resulting splitting is on the same order of magnitude in both material systems. Neglecting this parameter is therefore not suitable in the studied material system. By artificially varying Δ_{so}, we find a strongly linear correlation between the spin-orbit splitting and the energy difference between the first two hole states.

ACKNOWLEDGMENTS

The authors would like to thank Paul Gartner, Liverios Lymperakis, Patrick Rinke, and Frank Jahnke for fruitful discussions as well as Sixten Boeck and Christoph Freysoldt for support concerning the S/PHI/nX library. This work was supported by the Deutsche Forschungsgemeinschaft (research group "Physics of nitride-based, nanostructured, light-emitting devices," Projects No. Ne 428/6-3 and No. Cz 31/

14-3). S.S. was further supported by the Humboldt Foundation through Feodor-Lynen research. D.M., S.S., and G.C. also acknowledge a grant for CPU time from the NIC at the Forschungszentrum Jülich.

APPENDIX: EIGHT-BAND k·p HAMILTONIAN

In a basis set of eight complex wave functions

$$\Psi = (\psi^{\Gamma_6}_{-1/2}, \psi^{\Gamma_6}_{1/2}, \psi^{\Gamma_8}_{-3/2}, \psi^{\Gamma_8}_{-1/2}, \psi^{\Gamma_8}_{1/2}, \psi^{\Gamma_8}_{3/2}, \psi^{\Gamma_7}_{-1/2}, \psi^{\Gamma_7}_{-1/2}),$$

where Γ_6 denotes the conduction-band states, Γ_8 denotes the light- and heavy-hole valence-band states, and Γ_7 denotes the spin-orbit coupling, the eight-band $\mathbf{k}\cdot\mathbf{p}$ Hamiltonian[44] can be written as

$$\hat{H}^{8\times 8} = \begin{pmatrix} \hat{H}_c & \hat{H}_s \\ \hat{H}_s^\star & \hat{H}_v \end{pmatrix} = \begin{pmatrix} A & 0 & V^\star & 0 & \sqrt{3}V & -\sqrt{2}U & -U & \sqrt{2}V^\star \\ 0 & A & -\sqrt{2}U & -\sqrt{3}V^\star & 0 & -V & \sqrt{2}V & U \\ V & -\sqrt{2}U & -P+Q & -S^\star & R & 0 & \sqrt{\frac{3}{2}}S & -\sqrt{2}Q \\ 0 & -\sqrt{3}V & -S & -P-Q & 0 & R & -\sqrt{2}R & \frac{1}{\sqrt{2}}S \\ \sqrt{3}V^\star & 0 & R^\star & 0 & -P-Q & S^\star & \frac{1}{\sqrt{2}}S^\star & \sqrt{2}R^\star \\ -\sqrt{2}U & -V^\star & 0 & R^\star & S & -P+Q & \sqrt{2}Q & \sqrt{\frac{3}{2}}S^\star \\ -U & \sqrt{2}V^\star & \sqrt{\frac{3}{2}}S^\star & -\sqrt{2}R^\star & \frac{1}{\sqrt{2}}S & \sqrt{2}Q & -P-\Delta_{\mathrm{so}} & 0 \\ \sqrt{2}V & U & -\sqrt{2}Q & \frac{1}{\sqrt{2}}S^\star & \sqrt{2}R & \sqrt{\frac{3}{2}}S & 0 & -P-\Delta_{\mathrm{so}} \end{pmatrix}, \tag{A1}$$

where the effective mass and the six-band model can be found in the 2×2 $\hat{H}_c$ for the electron and the 6×6 $\hat{H}_v$ for the hole states. $\hat{H}_s$ denotes the superposition of electron and hole states within the eight-band model. The matrix elements are given as

$$A = E_{\mathrm{cb}} - \frac{\hbar^2}{2m_0}\gamma_c(\partial_x^2+\partial_y^2+\partial_z^2),$$

$$P = -E_{\mathrm{vb}} - \gamma_1\frac{\hbar^2}{2m_0}(\partial_x^2+\partial_y^2+\partial_z^2),$$

$$Q = -\gamma_2\frac{\hbar^2}{2m_0}(\partial_x^2+\partial_y^2-2\partial_z^2),$$

$$R = \sqrt{3}\frac{\hbar^2}{2m_0}[\gamma_2(\partial_x^2-\partial_y^2) - 2i\gamma_3\partial_x\partial_y],$$

$$S = -\sqrt{3}\gamma_3\frac{\hbar^2}{2m_0}\partial_z(\partial_x - i\partial_y),$$

$$U = \frac{-i}{\sqrt{3}}P_0\partial_z,$$

$$V = \frac{-i}{\sqrt{6}}P_0(\partial_x - i\partial_y). \tag{A2}$$

Note the minus sign appearing in the S instead of the R element in contrast to Ref. 44. The γ_i denote the modified Luttinger parameters and can be derived from the original Luttinger parameters γ_i^L by

$$\gamma_c = \frac{m_0}{m_e} - \frac{E_P}{3}\left(\frac{2}{E_g} + \frac{1}{E_g+\Delta_{\mathrm{so}}}\right),$$

$$\gamma_1 = \gamma_1^L - \frac{E_P}{3E_g+\Delta_{\mathrm{so}}},$$

$$\gamma_2 = \gamma_2^L - \frac{1}{2}\frac{E_P}{3E_g+\Delta_{\mathrm{so}}},$$

$$\gamma_3 = \gamma_3^L - \frac{1}{2}\frac{E_P}{3E_g+\Delta_{\mathrm{so}}}. \tag{A3}$$

E_{cb} and E_{vb} denote the unstrained conduction- and valence-band offsets; $E_g = E_{cb} - E_{vb}$ is the band gap. P_0 is the coupling parameter between conduction and valence bands, Δ_{so} denotes the spin-orbit coupling, and

$$E_P = 2m_0 \frac{P_0^2}{\hbar^2} \tag{A4}$$

is the Kane parameter.

*marquardt@mpie.de
†Present address: Tyndall National Institute, Lee Maltings, Prospect Row, Cork, Ireland.

[1] F. A. Ponce and D. P. Bour, Nature (London) **386**, 351 (1997).
[2] K. Kawasaki, D. Yamazaki, A. Kinoshita, H. Hirayama, K. Tsutsui, and Y. Aoyagi, Appl. Phys. Lett. **79**, 2243 (2001).
[3] K. Hoshino and Y. Arakawa, Phys. Status Solidi C **1**, 2516 (2004).
[4] M. Razeghi and A. Rogalski, J. Appl. Phys. **79**, 7433 (1996).
[5] S. Lazar, C. Hébert, and H. Zandbergen, Ultramicroscopy **98**, 249 (2004).
[6] F. Widmann, J. Simon, B. Daudin, G. Feuillet, J. L. Rouvière, N. T. Pelekanos, and G. Fishman, Phys. Rev. B **58**, R15989 (1998).
[7] J. Simon, N. T. Pelekanos, C. Adelmann, E. Martinez-Guerrero, R. André, B. Daudin, L. S. Dang, and H. Mariette, Phys. Rev. B **68**, 035312 (2003).
[8] V. A. Fonoberov and A. A. Balandin, J. Appl. Phys. **94**, 7178 (2003).
[9] N. Baer, S. Schulz, P. Gartner, S. Schumacher, G. Czycholl, and F. Jahnke, Phys. Rev. B **76**, 075310 (2007).
[10] S. V. Novikov, N. M. Stanton, R. P. Campion, R. D. Morris, H. L. Geen, C. T. Foxon, and A. J. Kent, Semicond. Sci. Technol. **23**, 015018 (2008).
[11] N. Gogneau *et al.*, Phys. Status Solidi C **1**, 1445 (2004).
[12] E. Martinez-Guerrero, C. Adelmann, F. Chabuel, J. Simon, N. T. Pelekanos, G. Mula, B. Daudin, G. Feuillet, and H. Mariette, Appl. Phys. Lett. **77**, 809 (2000).
[13] C. Adelmann *et al.*, Mater. Sci. Eng., B **82**, 212 (2001).
[14] B. Daudin *et al.*, Jpn. J. Appl. Phys., Part 1 **40**, 1892 (2001).
[15] J. P. Garayt *et al.*, Physica E (Amsterdam) **26**, 203 (2005).
[16] J. Seebeck, T. R. Nielsen, P. Gartner, and F. Jahnke, Eur. Phys. J. B **49**, 167 (2006).
[17] T. R. Nielsen, P. Gartner, M. Lorke, J. Seebeck, and F. Jahnke, Phys. Rev. B **72**, 235311 (2005).
[18] M. Grundmann, O. Stier, and D. Bimberg, Phys. Rev. B **52**, 11969 (1995).
[19] A. Wojs, P. Hawrylak, S. Fafard, and L. Jacak, Phys. Rev. B **54**, 5604 (1996).
[20] J.-J. Shi and Z.-Z. Gan, J. Appl. Phys. **94**, 407 (2003).
[21] C. Pryor, Phys. Rev. B **57**, 7190 (1998).
[22] O. Stier, M. Grundmann, and D. Bimberg, Phys. Rev. B **59**, 5688 (1999).
[23] A. D. Andreev and E. P. OReilly, Phys. Rev. B **62**, 15851 (2000).
[24] T. Saito and Y. Arakawa, Physica E (Amsterdam) **15**, 169 (2002).
[25] R. Santoprete, B. Koiller, R. B. Capaz, P. Kratzer, Q. K. K. Liu, and M. Scheffler, Phys. Rev. B **68**, 235311 (2003).
[26] S. Schulz and G. Czycholl, Phys. Rev. B **72**, 165317 (2005).
[27] L. W. Wang, J. Kim, and A. Zunger, Phys. Rev. B **59**, 5678 (1999).
[28] L. W. Wang, A. J. Williamson, A. Zunger, H. Jiang, and J. Singh, Appl. Phys. Lett. **76**, 339 (2000).
[29] G. Bester and A. Zunger, Phys. Rev. B **71**, 045318 (2005).
[30] H. Fu, L. Wang, and A. Zunger, Appl. Phys. Lett. **71**, 3433 (1997).
[31] J. W. Luo, S. S. Li, and J. B. Xia, Appl. Phys. Lett. **88**, 143108 (2006).
[32] N. Baer, P. Gartner, and F. Jahnke, Eur. Phys. J. B **42**, 231 (2004).
[33] A. D. Andreev and E. P. O'Reilly, Appl. Phys. Lett. **79**, 521 (2001).
[34] T. Saito and Y. Arakawa, Phys. Status Solidi C **0**, 1169 (2003).
[35] N. Baer, S. Schulz, S. Schumacher, P. Gartner, G. Czycholl, and F. Jahnke, Appl. Phys. Lett. **87**, 231114 (2005).
[36] S. Schulz, S. Schumacher, and G. Czycholl, Phys. Rev. B **73**, 245327 (2006).
[37] M. Winkelnkemper, A. Schliwa, and D. Bimberg, Phys. Rev. B **74**, 155322 (2006).
[38] S. Schulz, S. Schumacher, and G. Czycholl, Eur. Phys. J. B **64**, 51 (2008).
[39] D. M. Wood and A. Zunger, Phys. Rev. B **53**, 7949 (1996).
[40] J. C. Phillips, *Bonds and Bands in Semiconductors* (Academic, New York, 1973).
[41] D. J. Chadi, Phys. Rev. B **16**, 790 (1977).
[42] Y. C. Chang, Phys. Rev. B **37**, 8215 (1988).
[43] J. P. Loehr, Phys. Rev. B **50**, 5429 (1994).
[44] T. B. Bahder, Phys. Rev. B **41**, 11992 (1990).
[45] I. Vurgaftman and J. R. Meyer, J. Appl. Phys. **94**, 3675 (2003).
[46] O. Marquardt, S. Boeck, C. Freysoldt, T. Hickel, and J. Neugebauer (unpublished).
[47] http://www.sphinxlib.de
[48] P. Rinke, M. Winkelnkemper, A. Qteish, D. Bimberg, J. Neugebauer, and M. Scheffler, Phys. Rev. B **77**, 075202 (2008).
[49] D. Fritsch, H. Schmidt, and M. Grundmann, Phys. Rev. B **67**, 235205 (2003).
[50] J. Stanley and N. Goldsman, Phys. Rev. B **51**, 4931 (1995).
[51] F. Widmann, B. Daudin, G. Feuillet, Y. Samson, J. L. Rouvière, and N. T. Pelekanos, J. Appl. Phys. **83**, 7618 (1998).
[52] M. Arlery, J. L. Rouvière, F. Widmann, B. Daudin, G. Feuillet, and H. Mariette, Appl. Phys. Lett. **74**, 3287 (1999).
[53] P. Yu and M. Cardona, *Fundamentals of Semiconductors* (Springer, Berlin, 2001).
[54] S. Schulz, S. Schumacher, and G. Czycholl, Phys. Status Solidi B **244**, 2399 (2007).
[55] E. P. Pokatilov, V. A. Fonoberov, V. M. Fomin, and J. T. Devreese, Phys. Rev. B **64**, 245328 (2001).